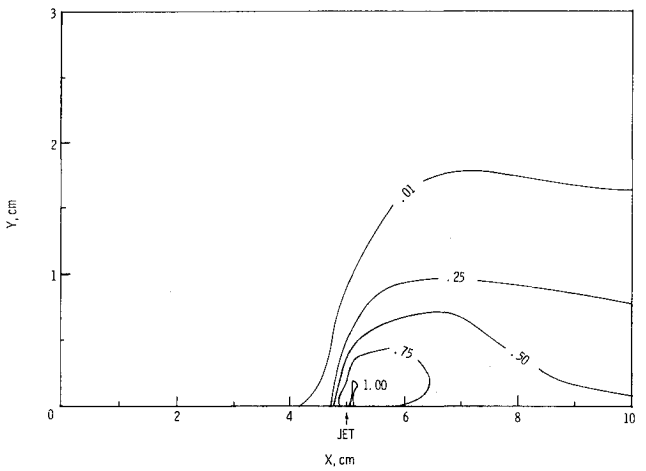

Fig. 3 Hydrogen mass fraction contours in lower half duct.

contour line lies at ¼ the duct height after proceeding only 5 slot widths downstream. The recirculating region upstream of the slot convects hydrogen forward of the jet, and the mixture goes from fuel lean to rich as the slot is approached. The separated flow downstream of the slot captures hydrogen, producing a very fuel rich region. These are phenomena that have been observed in experimental scramjet design, the upstream region providing a beneficial area for fuel ignition and the downstream region (being fuel rich) imposing an ignition problem.

Conclusions

A program has been developed to simulate the near sonic perpendicular injection of hydrogen into a ducted supersonic air stream. A case using actual conditions encountered in current scramjet design has been successfully analyzed, producing results that agree qualitatively with experimental observations. A modified form of a popular numerical damping scheme was employed to prevent numerical oscillations near shocks. The damping term was made proportional not only to the second derivative of pressure, but also the second derivative of temperature to produce a stable solution behind the hydrogen jet in the neighborhood of the recompression shock. Additionally, alternating boundary conditions were used to specify the wall density yielding a more physically realistic density field near the wall. A number of improvements and extensions still remain, however, none of which are trivial. First, the turbulence model must be improved to more adequately consider the complex flowfield that exists. Second, a chemistry model must be added to consider at least the H_2-air reaction that occurs; more complete finite rate modeling will likely require an implicit rather than explicit integrator. Finally the actual problem that must be considered is three- rather than two-dimensional, limiting implementation of this work to all but the largest current or future vector computers. The current effort does, however, represent a first attempt to numerically model the perpendicular fuel injector problem in the engine, and should provide guidance in the on going scramjet design effort at Langley Research Center.

References

[1] Jones, R. A. and Huber, P. W., "Toward Scramjet Aircraft," *Astronautics and Aeronautics*, Vol. 16, Feb. 1978, pp. 38-48.

[2] Pan, Y. S., "The Development of a Three-Dimensional Partially Elliptic Flow Computer Program for Combustor Research," NASA CR-3057, Nov. 1978.

[3] MacCormack, R. W. and Baldwin, B. S., "A Numerical Method for Solving the Navier-Stokes Equations with Application to Shock-Boundary Layer Interactions," AIAA Paper 75-1, 1975.

[4] Cebeci, T. and Smith, A.M.O., *Analysis of Turbulent Boundary Layers*, Academic Press, New York, pp. 170-173.

Asymmetry of a Circular Jet Observed in Near and Far Fields

Kingo Yamamoto*
State University of New York at Buffalo, Buffalo, N. Y.
and
Roger E.A. Arndt†
University of Minnesota, Minneapolis, Minn.

Introduction

An extensive survey of the turbulence characteristics and the acoustic field of low Reynolds number jets has been recently completed. One of the unexpected findings was that slight but detectable asymmetries exist in both the flowfield and the surrounding acoustic field.

During preliminary testing, the true jet axis was determined with a single hot-film probe. The aerodynamic jet axis is defined as the locus of points in the flow at which the turbulence intensity is a minimum. Measurements were made at 10 equally spaced X stations between $X=D$ and $X=10D$ from the jet exit plane. The results show that at each X station the deviation from the geometrical jet axis was on the order of 2-4% of the nozzle diameter, and the true jet axis has the form of a helical wave. This helical wavelike jet axis was observed in three different jets of 12.7, 6.35, and 3.18-mm diameter. It was further confirmed that rotating of the nozzle or settling chamber does not give any noticeable effect on the profile of the true jet axis and that this profile changed significantly from one day to another. This may indicate that the helical wavelike disturbances are generated far upstream of the nozzle. One may speculate that since the turbulence is more sensitive to the variations of flow conditions than is the mean flow, the asymmetry of jet flow is more easily observed in turbulence intensity measurements. In fact, this was clearly confirmed in the present investigation. It is interesting to note that the asymmetry of the jet flow was observed not only in the flowfield but also in the radiated field. It should be added that the circumferential asymmetry of the sound pressure level was more strongly observed in the sideline noise signature than at observation angles close to the jet axis.

Measurements

Turbulence intensity measurements were made in three different sized jets at various Mach numbers. Figure 1 contains an example of the resulting data obtained in a 12.7-mm jet at a Mach number, M, of 0.297. These data represent the measured axial component of turbulence measured at various axial and radial positions. A single hot-film probe was traversed radially across the jet at distances of $Z=\pm 3D$ from the centerline. The measurements were made at equally spaced axial stations ranging from 1-10 diameters from the plane of the nozzle.

The turbulence intensity attains a maximum value near $Z/D=0.5$ at any downstream station. The asymmetry of the profiles is evident. This asymmetry of the jet flow is not due to the nozzle configuration. This was confirmed by rotating the nozzle by 180 deg, yielding the same results. It is debatable whether these results imply a natural asymmetry of the flow due to a helical mode in the jet turbulence or upstream flow

Received Oct. 25, 1978.

Index category: Aeroacoustics.

*Assistant Professor of Research, Dept. of Aerospace Engineering.
†Professor and Director of St. Anthony Falls Hydraulic Laboratory. Member AIAA.

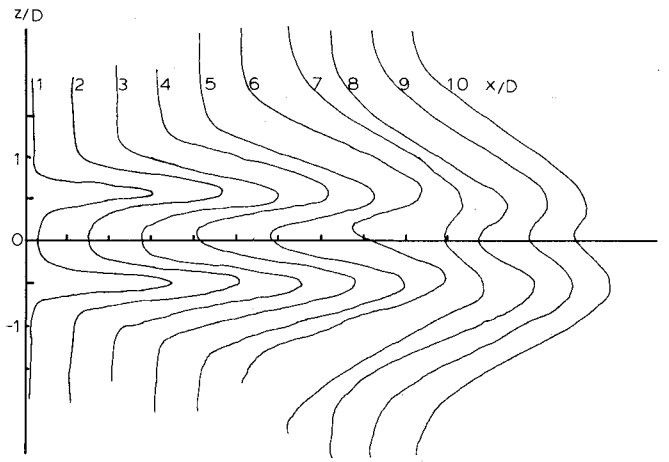

Fig. 1 Turbulence u-component profiles at various downstream locations for the 12.7-mm jet at $M = 0.297$.

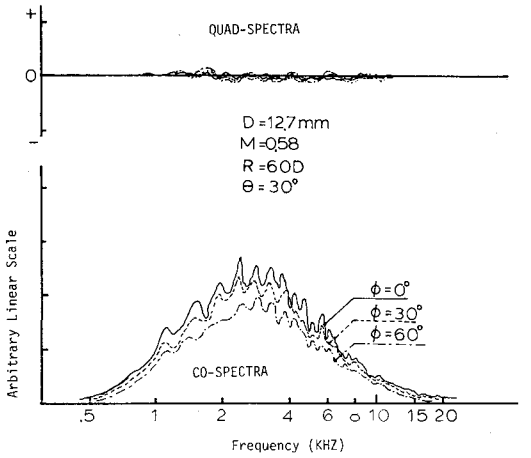

Fig. 3 Cross spectral density of jet noise at various axiumthal locations.

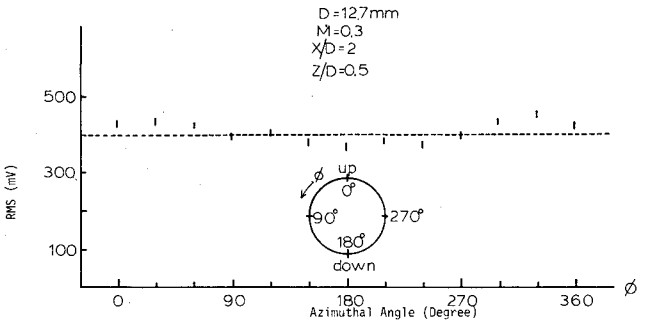

Fig. 2 Circumferential distribution of rms voltage of fluctuating velocity signals (u component).

conditions. We note in Fig. 1 that the turbulence intensity on the jet axis grows almost linearly up to 5-diam downstream, and the intensity approximately doubles over an increment of 1 diameter. The asymmetry of the turbulence intensity is evident and was observed in all of the three jets of 12.7, 6.35, and 3.1-mm diameter, respectively. As shown in Fig. 1, the variation between the peak intensity observed in the lower and the upper mixing layers seems to grow gradually up to 5-diam downstream and then to decay slowly with a further increase of downstream distance. A similar asymmetry of the turbulence intensity in a supersonic jet was reported by McLaughlin et al.[1]

To explore further the asymmetry of the circular jet, a measurement of the circumferential distribution of rms fluctuating velocity signals was undertaken. A hot-wire (DISA 55P11) probe was rotated in the plane vertical to the true jet axis at $X/D=1$. The sensor portion of the probe remained in a horizontal position during rotation along a circle of radius $0.5D$. The results of this experiment are shown in Fig. 2 where the ordinate represents linearized output voltage of the hotwire and the abscissa corresponds to the azimuthal angle (degrees). Here we note a somewhat sinusoidal profile centered at the 400-mV line. The results, however, must be interpreted carefully. The hot-wire sensor whose length and diameter are 1.25 mm and 5 μm, respectively, can be thought to be completely immersed in the very thin mixing layer when the sensor probe is located at $\phi = 0$ deg and 180 deg. With increasing azimuthal angle, ϕ, the sensor wire will cut the mixing layer at larger angles, and at $\phi = 90$ deg and 270 deg, the wire is aligned radially across the mixing layer. At this position the spatial averaging effect should be a maximum. If we assume that the sinusoidal profile of the turbulence (u component) is only due to the averaging effect of the hot wire, then we should have a minimum at $\phi = 90$ deg and 270 deg. However, this is not consistent with the observations in Fig. 2. Here the minimum output voltage is observed at about $\phi = 180$ deg. It is now obvious that even for a circular jet the turbulence intensity (u component) is not axisymmetric, and a jet flow may be speculated to have a helical structure to some extent in the downstream direction. This asymmetry of the flow has a noticeable effect on the radiated field.

As a part of the present study, circumferential cross correlation measurements were conducted which were aimed at providing data to verify the validity of Michalke's spectral theory.[2] Two B&K 6.35-mm microphones were located at 60 jet diameters away from the center of the jet exit plane with a 30-deg inclination from the jet axis. A microphone was rotated from 0 deg to 360 deg along a circle of radius 30 jet diameters which is vertical to the jet axis. At each 15-deg increment of azimuthal angle, the signals from the two microphones were cross correlated.

During preliminary testing, two sets of B&K microphones were carefully phased-matched. In the frequency range between 1,000 and 10,000 Hz the observed phase lag was within ± 2 deg. After the two microphones were positioned for circumferential cross-correlation measurements as previously described, a B&K sound level calibrator (type 4230) was located on the geometrical jet axis. With this setup we confirmed that the signals from the two microphones produced phase-lag within $\pm$ 2.5 deg at each 15-deg increment of azimuthal separation angle between 0 deg and 360 deg at 1,000 Hz. Figure 3 illustrates the cross spectral densities of jet noise plotted frequency in the range of 500 to 20,000 Hz for the first three azimuthal separation angles. Here we see a definite phase-lag between the two signals. The maximum phase-lag observed was 7 deg. It should be noted that the asymmetry of the radiated noise is more strongly observed in the lateral direction ($\theta = 90$ deg) than in the axial direction. This was confirmed by circumferential cross-correlation measurements at $\theta = 90$ deg (data are not reported herein). In this case it was observed that the high-frequency portion of the spectrum of radiated sound changed its shape with azimuthal separation angle. On the other hand, the low-frequency remained the same at any azimuthal separation angle. It is likely that convection effects smooth out the circumferential irregularity of radiated sound.

Conclusion

In summary, one may say that our findings of an asymmetry of a circular jet indicates that even a very carefully designed circular nozzle can produce nonaxisymmetry in both flow and acoustic quantities, particulaly at low Reynolds numbers. This situation would require one to pay particular

attention to the interpretation of low Reynolds number jet data.

Acknowledgment

This work was supported by NASA Lewis Research Center and the U.S. Air Force, Office of Scientific Research.

References

[1] McLaughlin, D.K., Morrison, G.L., and Troutt, T.R., *Journal of Fluid Mechanics*, Vol. 69, Pt. 1, May 1975, pp. 73-95.

[2] Michalke, A., "A Wave Model for Sound Generation in Circular Jets," DLR FB 70-57, 1970, Deutsche Forschungs-und Versuchsanstalt fur Luft- und Raumfahrt, Institut fur Turbulenzforschung, Berlin, W. Germany, 1970.

Elastic Beams of Various Orders

James Ting-Shun Wang*
Georgia Institute of Technology, Atlanta, Ga.
and
John N. Dickson†
Lockheed-Georgia Company, Marietta, Ga.

General Theory

THE geometry, coordinate system, and some symbols are shown in Fig. 1. Plane state of stress in a homogeneous and isotropic beam of unit width subjected to loading

$$q = q_x(x)i + q_y(x)j \tag{1}$$

along $y=h$ is considered for establishing the general theory. The plane region A is bounded within $-L_1 \le x \le L_2$ and $0 \le y \le h$ by the boundary line S. Pertinent equations based on linear elasticity theory are listed below, and tensor notation is used for the convenience of presentation:

$$\iint \sigma_{ji,j}\delta u_i \mathrm{d}A + \int (\bar{T}_i - \sigma_{ji}n_j)\delta u_i \mathrm{d}S = 0 \tag{2}$$

$$\sigma_{ij} = \frac{E}{1-\nu^2}[\nu e_{kk}\delta_{ij} + (1-\nu)e_{ij}] \tag{3}$$

$$e_{ij} = \tfrac{1}{2}(u_{i,j} + u_{j,i}) \tag{4}$$

where σ_{ij} and e_{ij} for i and j ranging from 1 to 2 are the stress and strain tensors. $\bar{T}_i$ is the surface traction at the boundary line with unit outward normal vector n_j. The modulus of elasticity, Poisson's ratio, shear modulus, and displacements are E, ν, G, and u_i, respectively. Equations (2-4) may be found in standard text books on mechanics of solids such as Refs. 1-3. It is clear that the first part of Eq. (2) involves the Euler's equations which are the equilibrium equations, and the second part contains the boundary conditions. The longitudinal displacement, $u_1 = u$, and the transverse displacement, $u_2 = w$ are represented by power series,

$$u = \sum_{m=0}^{\infty} U_m(x)y^m, \quad w = \sum_{m=0}^{\infty} W_m(x)y^m \tag{5}$$

Received June 15, 1978; revision received Jan. 8, 1979.

Index category: Structural Statics.

*Professor, School of Engineering Science and Mechanics.

†Aircraft Development Engineer, Specialist, Advanced Structures Dept. Member AIAA.

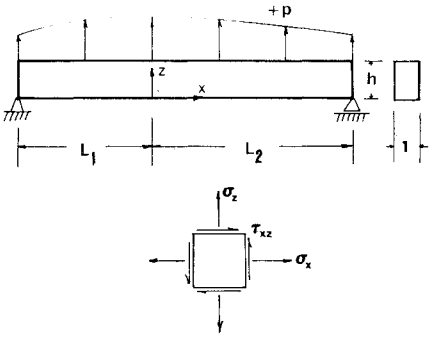

Fig. 1 Geometry, coordinates, and sign convention.

By substituting Eq. (5) into equilibrium equations contained in Eq. (2), and collecting like terms of y, one obtains the following recurrence relations:

$$U_{m+2} = -\frac{1}{(1-\nu)(m+2)}\left[(1+\nu)W'_{m+1} + \frac{2}{m+1}U''_m\right] \tag{6}$$

$$W_{m+2} = -\frac{1}{2(m+2)}\left[(1+\nu)U'_{m+1} + \frac{1-\nu}{m+1}W''_m\right] \tag{7}$$

where the prime denotes differentiation with respect to x. The free-of-stress boundary conditions along $y=0$ require

$$U_1 = -W'_0, \quad W_1 = -\nu U'_0 \tag{8}$$

Consequently, all of the unknown coefficients for displacements shown in Eq. (5) can be expressed in terms of U_0 and W_0 and their derivatives. They may be written in the following general form:

$$\begin{Bmatrix} U_m \\ W_m \end{Bmatrix} = \begin{bmatrix} g_{mw} & g_{mu} \\ k_{mw} & k_{mu} \end{bmatrix} \frac{\mathrm{d}^m}{\mathrm{d}x^m} \begin{Bmatrix} W_0 \\ U_0 \end{Bmatrix} \tag{9}$$

in which $g_{mw} = k_{mu} = 0$ if m is an even integer, and $g_{mu} = k_{mw} = 0$ if m is an odd integer. Since g_{mw} and g_{mu} do not exist at the same time, a single symbol g_m will be used subsequently in place of g_{mw} and g_{mu}. Similarly, k_m will be used in place of k_{mw} and k_{mu}. The first few g_m and k_m are listed in Table 1. The stress components σ_x, τ_{xy} and σ_y can now be represented in power series of y with coefficients related to derivatives of U_0 and W_0,

$$\sigma_x = \sum_{i=0}^{I} \sigma_{xi}y^i = E(U'_0 - yW''_0 - y^2U'''_0 + \frac{1}{3}y^3W'^{v}_0 + \ldots) \tag{10}$$

$$\tau_{xy} = \sum_{j=0}^{J} \tau_{xyj}y^j = E(-yU''_0 + \frac{1}{2}y^2W'''_0 + \frac{1}{3}y^3U'^{v}_0 - \frac{1}{12}y^4W^{v}_0 + \ldots) \tag{11}$$

$$\sigma_y = \sum_{k=0}^{K} \sigma_{yk}y^k = \frac{E}{2}(y^2U'''_0 - \frac{1}{3}y^3W'^{v}_0 - \frac{1}{6}y^4U^{v}_0 + \frac{1}{30}y^5W^{v\prime}_0 + \ldots) \tag{12}$$

By satisfying the boundary conditions along $y=h$ contained in the second part of Eq. (2),

$$\tau_{yx} = q_x(x) \text{ and } \sigma_y = q_y(x) \tag{13}$$